

# Flute instability of an ion-focused slab electron beam in a broad plasma

David H. Whittum

*National Laboratory for High Energy Physics (KEK), 1-1 Oho, Tsukuba, Ibaraki 305, Japan*

Martin Lampe, Glenn Joyce, and Steven P. Slinker

*Naval Research Laboratory, Washington, D.C. 20375*

Simon S. Yu and William M. Sharp

*Lawrence Livermore National Laboratory, University of California, Livermore, California 94550*

(Received 7 July 1992)

An intense relativistic electron beam with an elongated cross section, propagating in the ion-focused regime through a broad, uniform, unmagnetized plasma, is shown to suffer a transverse flute instability. This instability arises from the electrostatic coupling between the beam and the plasma electrons at the ion-channel edge. The instability is found to be absolute and the asymptotic growth of the flute amplitude is computed in the “frozen-field” approximation and the large skin-depth limit. The minimum growth length is shown to be much less than the betatron period, with the consequence that focusing is rendered ineffective. It is further shown that growth is much reduced when the beam propagates through a narrow channel where the ion density greatly exceeds that of the surrounding plasma. In this limit, a modest spread in betatron frequency produces rapid saturation. The effect of plasma electron collisions is also considered. Results of beam breakup simulations are noted.

PACS number(s): 41.75.Fr, 52.40.Mj, 52.35.Py, 52.50.Gj

## I. INTRODUCTION

The “ion-focused” regime [1,2] (IFR) of transport for intense relativistic electron beams typically refers to propagation in a narrow plasma channel which is less dense than the beam core (“underdense”). All plasma electrons are expelled to large radii or to the beam pipe, and the remaining ion column provides the strong focusing required to transport intense beams over long distances. In this form IFR transport has been employed experimentally with great success to exceed the limitations of conventional magnetic focusing [3–8].

However, in some proposed applications of the IFR, the plasma channel may be much broader than the beam, or may be surrounded by a broad region of lower density plasma. For example, applications of the IFR (including focusing [9,10], emittance damping [11], and acceleration [12,13]) have been proposed for beams typical of an electron-positron collider [14], i.e., a pulse length  $T \sim 1\text{--}10$  ps, peak current  $I \sim 0.1\text{--}10$  kA, and a spot size  $a \sim 1\text{--}1000$  nm, with plasma densities in the range  $n_p \sim 10^{15}\text{--}10^{20}$  cm $^{-3}$ . In this extreme parameter range, rapid ionization of the gas by the beam and secondary electrons can lead to the formation of a *broad* ionized region [15]. As another example, recent experimental work by Miller *et al.* [16] has focused on the propagation of a 1.7-MeV, 1-kA, 10-ns beam in a laser-created underdense channel embedded in a *broad* discharge plasma, with  $n_p \sim 10^9$  cm $^{-3}$ . In these examples the plasma may still be sufficiently tenuous that no plasma electrons remain *within the beam volume* and one may rightly refer to the focusing as ion focusing. However, the pure ion channel is surrounded by a quasineutral plasma. Recently [17,18]

we have shown that a *cylindrical* beam injected into a broad plasma channel of uniform density is subject to a dipole transverse two-stream instability [19,20] (“electron hose”) with growth length less than a betatron wavelength.

In this work we show that an ion-focused *slab* beam, while stable against plasma electron-coupled dipole perturbations, is subject to a rapidly growing *flute* instability, analogous in character to the electron-hose instability. As for the cylindrical beam, the minimum growth length is less than a betatron wavelength. This transverse two-stream instability seriously complicates use of the IFR for the intense asymmetric beams typical of high-energy applications.

In Sec. II two coupled equations are derived, describing the linear evolution of the flute instability for a slab beam in a uniform underdense collisionless plasma. The dispersion relation is examined, and asymptotic growth is calculated. The result is shown to be disastrously unstable. In Sec. III we go on to show that growth may be greatly reduced when the ion density is peaked on axis. Results of beam breakup simulations are noted. In Sec. IV we include the effect of plasma-electron collisions and note the condition for stability resulting from the combined effects of collisions and a distributed betatron resonance. In Sec. V a discussion and conclusions are offered. Calculations of asymptotic forms are detailed in the Appendix.

## II. TRANSPORT IN A BROAD COLLISIONLESS PLASMA

First, we summarize our approximations. We assume that the beam current varies at most adiabatically on the

time scale for electron-plasma oscillations, i.e.,  $\omega_p T_r \gg 1$ , where  $\omega_p$  is the plasma-electron frequency,  $\omega_p^2 = 4\pi n_p e^2 / m$ ,  $m$  is the electron mass,  $-e$  is the electron charge, and  $T_r$  is the current rise time. The initial plasma density  $n_p$  is assumed to be uniform and underdense, i.e.,  $n_p < n_b$ , where the beam density on axis is  $n_b$  and is a function of  $\tau = t - z/V_b$ , where  $t$  is time and  $z$  is axial displacement. The beam axial velocity is  $V_b \sim c$ , with  $c$  the speed of light. In this limit, plasma electrons are adiabatically expelled from a slab volume ("ion channel") of width  $2b \sim 2a(n_b/n_p)$ , where  $2a$  is the beam width, as depicted in Fig. 1 [21]. We will neglect ion motion, and this entails the assumption that  $\omega_i T \ll 1$ , where  $T$  is the beam duration and  $\omega_i$  is the ion plasma frequency, and  $\omega_i^2 = 4\pi n_p e^2 / m_i$ , with  $m_i$  the ion mass. This also entails neglect of the more rapid "slosh" motion of the strongly focused ions near the beam. Thus, we assume  $\omega_s T \ll 1$ , where the slosh angular frequency  $\omega_s$  is given by  $\omega_s^2 \equiv 4\pi e^2 n_b / m_i$ . We further assume a large collisionless plasma skin depth,  $k_p^{-1} \equiv c/\omega_p \gg b$ . In this limit the axial plasma-electron current may be neglected. Finally, we impose the Budker or ion-focusing condition [1] on the plasma density,  $n_p \gg n_b/\gamma^2$ , where  $mc^2\gamma$  is the beam energy. The Lorentz-force equation then shows that beam electrons undergo transverse oscillations with betatron wave number

$$k_\beta = \frac{k_p}{\gamma^{1/2}}. \quad (1)$$

With these assumptions, the equilibrium plasma-electron charge density is

$$\rho_{e0} = -en_p [H(y-b) + H(-y-b)].$$

We take the beam charge density to be

$$\rho_{b0} = -en_b H(a-y)H(y+a),$$

with  $H$  the step function. (This choice is for convenience only, since the results are independent of the form of  $\rho_{b0}$ , provided it is confined to the channel.)

#### A. Coupled flute equations

We consider next the effect of a perturbation to the beam centroid in the form of a small displacement  $\xi(x)$  in

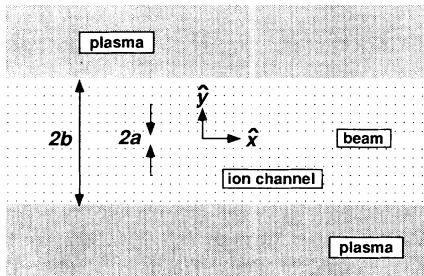


FIG. 1. In equilibrium, a relativistic electron beam of width  $2a$  propagates in the  $z$  direction (out of the page) through a channel of unneutralized ions. Plasma electrons have been expelled to  $|y| \geq b$ .

the  $y$  direction, as depicted in Fig. 2. The perturbation to the beam charge density is then

$$\rho_{b1} = -en_b \xi [\delta(a-y) - \delta(a+y)].$$

Maxwell's equations in the Lorentz gauge are

$$\left\{ \nabla_\perp^2 + \frac{\partial^2}{\partial z^2} - \frac{1}{c^2} \frac{\partial^2}{\partial t^2} \right\} \psi = 4\pi \rho_{e1}, \quad (2)$$

$$\left\{ \nabla_\perp^2 + \frac{\partial^2}{\partial z^2} - \frac{1}{c^2} \frac{\partial^2}{\partial t^2} \right\} A_z = -4\pi \rho_{b1}, \quad (3)$$

where  $A_z$  is the perturbed axial vector potential and  $\psi \equiv A_z - \phi$  is the "pinch potential," with  $\phi$  the perturbed scalar potential. We compute these potentials in the "frozen-field" approximation, in which the D'Alembertian is replaced by the transverse Laplacian  $\nabla_\perp^2$  and radiative effects are neglected. In addition, there is a transverse vector potential which may be neglected in the frozen-field approximation and provided  $\nabla_\perp \gg k_p$  (just the large skin-depth approximation).

The perturbed plasma-electron charge density  $\rho_{e1}$  is determined from the potentials through the electron cold-fluid equations

$$\frac{\partial \rho_{e1}}{\partial t} + \nabla_\perp \cdot (\rho_{e0} \mathbf{V}_e) \approx 0, \quad (4)$$

$$\frac{\partial \mathbf{V}_e}{\partial t} \approx \frac{e}{m} \nabla_\perp \phi, \quad (5)$$

where  $\mathbf{V}_e$  is the plasma-electron velocity. From Eqs. (4) and (5) it is straightforward to show that in the linearized small-amplitude limit,  $\rho_{e1}$  consists entirely of surface charge layers at  $y = \pm b$ . Thus,

$$\rho_{e1} = en_p \eta [\delta(b-y) - \delta(b+y)],$$

where  $\eta(x)$  describes the displacement of the channel wall.

To solve Eqs. (2) and (3), we change variables from  $z, t$  to  $z, \tau$  and Fourier transform in  $x$ , so that

$$\xi(z, \tau, x) \rightarrow \xi(z, \tau, k_x) \exp(ik_x x).$$

For brevity, we suppress notation distinguishing quantities,  $\xi, \eta$ , etc., from their Fourier transforms. In terms of

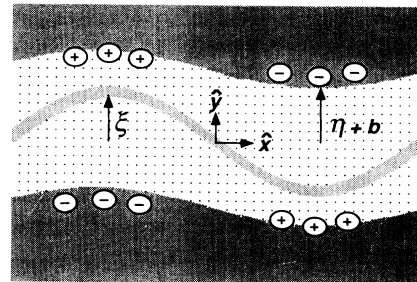


FIG. 2. A beam slice in the ion channel is displaced by an amount  $\xi(x)$  in the  $y$  direction, inducing a displacement  $\eta(x)$  of the channel wall. This image "flute" then deforms follow-on portions of the beam, resulting in instability.

$\xi$ ,  $\eta$ , and  $k_x$  (assumed positive, i.e.,  $k_x \rightarrow |k_x|$ ), the potentials are

$$A_z = -\frac{4\pi en_b \xi}{k_x} \times \begin{cases} \exp(-k_x a) \sinh(k_x y), & 0 < y < a \\ \exp(-k_x y) \sinh(k_x a), & a < y \end{cases} \quad (6)$$

$$\psi = -\frac{4\pi n_p e \eta}{k_x} \times \begin{cases} \exp(-k_x b) \sinh(k_x y), & 0 < y < b \\ \exp(-k_x y) \sinh(k_x b), & b < y \end{cases} \quad (7)$$

The linearized cold-fluid equations may then be expressed as

$$\left[ \frac{\partial^2}{\partial \tau^2} + \Omega_p^2(k_x) \right] \eta = \omega_p^2 k_x b e^{-k_x b} \xi, \quad (8)$$

where

$$\Omega_p^2(k_x) = \frac{1}{2} \omega_p^2 (1 - e^{-2k_x b}) \quad (9)$$

and  $k_x a \ll 1$  is assumed. Thus,  $\eta$  responds as a simple harmonic oscillator with characteristic angular frequency  $\Omega_p$  to the electrostatic field of the beam.

The Lorentz-force law for the beam is

$$\left[ \frac{\partial}{\partial z} \gamma \frac{\partial}{\partial z} + \gamma k_\beta^2 \right] \xi = k_p^2 \eta e^{-k_x b}. \quad (10)$$

This describes the deformation of the ion-focused beam by the plasma-electron image polarization on the ion-channel wall. Equations (8) and (10) provide a complete description of the linear evolution of the flute instability.

### B. Asymptotic growth

For an infinite beam and beam line taking a perturbation varying as  $\xi \propto \exp(ik_z z - i\omega \tau)$ , Eqs. (8) and (10) may be combined to yield the dispersion relation

$$\left[ 1 - \frac{\omega^2}{\Omega_p^2} \right] \left[ 1 - \frac{k_z^2}{k_\beta^2} \right] = \Delta^2(k_x b), \quad (11)$$

where

$$\Delta^2(\rho) = \frac{2\rho e^{-2\rho}}{1 - e^{-2\rho}} \quad (12)$$

and  $\rho \equiv k_x b$ . This is the general form of the cold-beam single-mode beam breakup dispersion relation, and, in the limit of small  $\rho$ ,  $\Delta^2 \rightarrow 1$ , so that Eq. (11) is identical to the familiar cold-beam two-stream dispersion relation [22,23]. In general the system is unstable for real  $\omega$  such that  $1 - \Delta^2 < \omega^2/\Omega_p^2 < 1$ , or real  $k_z$  such that  $1 - \Delta^2 < k_z^2/k_\beta^2 < 1$ . The growth rates go to infinity for  $\omega^2 \rightarrow \Omega_p^2$ , or  $k_z^2 \rightarrow k_\beta^2$  from below, and the result is an instability which is absolute in both the beam and lab frames [24–26]. Growth vanishes in the limit  $k_x \rightarrow 0$  corresponding to a rigid dipole displacement of the beam centroid. This is expected since the field of a one-dimensional dipole vanishes outside the source.

The asymptotic variation in  $z$  and  $\tau$  can be determined from a saddle-point analysis proceeding from Eq. (11) [24]. Alternatively, it is instructive to combine Eqs. (8) and (10) to obtain a single “beam breakup” equation [27]

for the flute amplitude alone:

$$\left[ \frac{\partial}{\partial z} \gamma \frac{\partial}{\partial z} + \gamma k_\beta^2 \right] \xi(z, \tau, k_x) = \int_0^\tau ds' W(k_x, \tau - \tau') \xi(z, \tau', k_x). \quad (13)$$

The Green’s function or “transverse wake” [28] is

$$W(k_x, \tau) = W(k_x) \sin[\Omega_p(k_x) \tau], \quad (14)$$

with amplitude [29]

$$W(k_x) = \frac{c^2 k_p^4 k_x b e^{-2k_x b}}{\Omega_p(k_x)}. \quad (15)$$

Equation (13) can be solved as an initial-value problem by Laplace transform, and the resulting integral can be evaluated by steepest descents in various limits. We take initial conditions

$$\xi(z=0, \tau, k_x) \approx \tilde{\xi}(k_x) H(\tau) \quad (16)$$

and consider two limits, summarizing the results of calculations given in the Appendix.

In the long-pulse limit,

$$\frac{\Omega_p \tau}{k_\beta z} \gg \Delta, \quad (17)$$

and the flux envelope varies as

$$\xi(z, \tau, k_x) \approx \tilde{\xi}(k_x) \frac{2^{1/2}}{3^{5/4} \pi^{1/2}} \frac{A_1^{1/2}}{\Omega_p \tau} e^{A_1} \times \sin\{\Omega_p \tau - 3^{-1/2} A_1 - \pi/12\}, \quad (18)$$

where the exponent is

$$A_1 = \frac{3^{1/2}}{4} \{\Delta^2(k_\beta z)^2 (\Omega_p \tau)\}^{1/3} \approx 0.92 \Gamma_1^{2/3} (k_\beta z)^{2/3} (\omega_p \tau)^{1/3}. \quad (19)$$

This may be expressed in terms of a characteristic growth length as  $A_1 = (z/L_1)^{2/3}$ , where

$$L_1 = \frac{2^3}{3^{9/4}} \left[ \frac{\gamma}{W(k_x) \tau} \right]^{1/2} \approx 0.18 \frac{\lambda_\beta}{(\omega_p \tau)^{1/2}} \frac{1}{\Gamma_1(k_x b)}. \quad (20)$$

The  $k_x$  dependence is subsumed in

$$\Gamma_1(\rho) = 2\{1 - \exp(-2\rho)\}^{-1/4} \rho^{1/2} \exp(-\rho), \quad (21)$$

as depicted in Fig. 3. Here,  $\lambda_\beta = 2\pi/k_\beta$  is the betatron period. Equation (17) corresponds to  $\Omega_p \tau \gg A_1 \gg 1$ . This result is essentially the “long-pulse, weak-focusing” limit familiar from beam breakup theory [30] or the “weak-beam” limit in two-stream theory. The maximum growth rate  $\Gamma_1 \sim 1$ , occurs at  $k_x b \sim 0.322$ , and this corresponds to a resonant flute frequency  $\Omega_p \sim 0.49\omega_p$  and minimum growth length

$$L_1 \sim 0.2 \lambda_\beta / (\omega_p \tau)^{1/2} \ll \lambda_\beta.$$

Thus, while a beam flute perturbation is *focused* by the

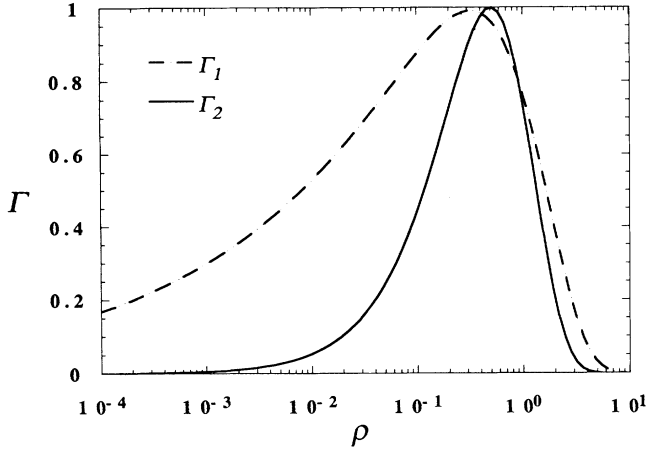


FIG. 3. Depicted are the normalized growth rates  $\Gamma_1$  and  $\Gamma_2$  of Eqs. (21) and (26) vs  $\rho = |k_x|b$ , the normalized flute wave number. All quantities are dimensionless. The maximum growth rate  $\Gamma_1 \sim 1$  occurs for  $\rho \sim 0.322$ , while the maximum  $\Gamma_2 \sim 1$  for  $\rho = \frac{1}{2}$ , corresponding to flute wavelengths  $\lambda_x = 2\pi/k_x \sim 19.5b$  and  $\lambda_x = 12.6b$ , respectively.

overlapping ion slab, it is more strongly destabilized by the distant plasma sheath.

A second limit, the long-range limit, corresponds to  $k_\beta z \gg \Omega_p \tau$ , or

$$\frac{k_\beta z}{\Omega_p \tau} \gg \frac{1}{\Delta}, \quad (22)$$

and in this limit the asymptotic growth varies as

$$\xi(z, \tau, k_x) \approx \tilde{\xi}(k_x) \frac{3^{1/4}}{2^{3/2} \pi^{1/2}} A_2^{-1/2} e^{A_2} \times \cos \left\{ k_\beta z - 3^{-1/2} A_2 + \frac{\pi}{12} \right\}, \quad (23)$$

where the exponent

$$A_2 = \frac{3^{3/2}}{4} \{ \Delta^2 (k_\beta z) (\Omega_p \tau)^2 \}^{1/3} \approx 0.74 \Gamma_2^{1/3} (k_\beta z)^{1/3} (\omega_p \tau)^{2/3}. \quad (24)$$

This may also be expressed as  $A_2 = (z/L_2)^{1/3}$ , where the growth length

$$L_2 = \frac{2^6}{3^{9/2}} \frac{\gamma k_\beta}{W(k_x) \Omega_p(k_x) \tau^2} \approx 0.39 \frac{\lambda_\beta}{(\omega_p \tau)^2} \frac{1}{\Gamma_2(k_x b)}. \quad (25)$$

The dependence on flute wave number is given by

$$\Gamma_2(\rho) = 2\rho \exp(1 - 2\rho), \quad (26)$$

which has maximum  $\Gamma_2 \sim 1$ , at  $\rho = \frac{1}{2}$ , as depicted in Fig. 3. The corresponding resonance occurs at  $\Omega_p \sim 0.56\omega_p$ . Equation (22) corresponds to  $A_2 \gg \Omega_p \tau$ . This is essentially the limit considered by Chao, Richter, and Yao [31].

To check these results, we solve Eq. (13) by standard numerical techniques [32]. The “exact” numerical solu-

tions in the long-range and long-pulse limits are depicted in Fig. 4, for  $\rho \sim 0.3$ . From this figure one can clearly discern the dominance of the betatron resonance for large  $k_\beta z / \Omega_p \tau$  and the plasma resonance for large  $\Omega_p \tau / k_\beta z$ . More precise comparisons of the analytic forms with numerical results are given in the Appendix.

With solutions in hand, one may check the approximations. A detailed analysis shows that neglect of the transverse vector potential is a fair approximation provided that

$$\frac{1}{ck_x^2} \frac{\partial^2 \xi}{\partial \tau \partial z}, \quad \frac{b}{ck_x} \frac{\partial^2 \xi}{\partial \tau \partial z} \ll \xi. \quad (27)$$

For  $k_x b \sim O(1)$ , these constraints are equivalent, and Eq. (27) may be rewritten as

$$k_p b / (2\gamma)^{1/4} \ll (k_\beta z / \omega_p \tau)^{1/6}.$$

It is not hard to show that this is also the condition for the frozen-field approximation. For typical applications,  $\omega_p \tau < 10^6$ , while  $z > \lambda_\beta$ , so that  $k_p b / (2\gamma)^{1/4} \ll 0.1$  is required. This is consistent with the large skin-depth approximation and is particularly well satisfied for  $\gamma \gg 1$ .

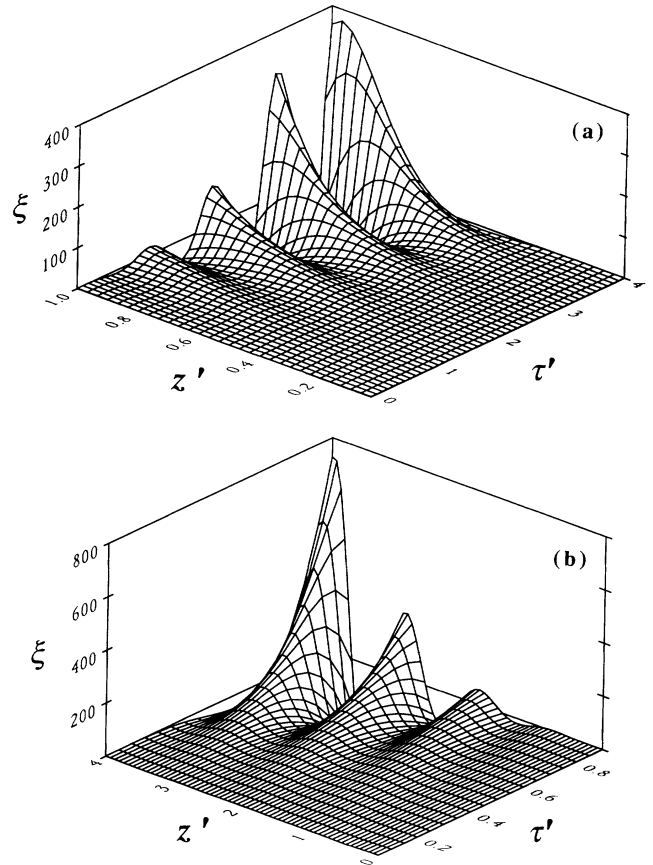


FIG. 4. Depicted are the two regimes of evolution for the beam flute amplitude in a broad plasma, corresponding to (a) a long pulse  $\Omega_p \tau > k_\beta z$ , where the resonance at  $\Omega_p$  is clearly evident, and (b) a long-range  $k_\beta z > \Omega_p \tau$ , where the resonance at  $k_\beta$  dominates. The axes are labeled in units of the flute and betatron periods,  $\tau' = \Omega_p \tau / 2\pi$  and  $z' = k_\beta z / 2\pi$ . Here,  $k_x b \sim 0.3$ .

For typical parameters of interest,  $\omega_p \tau > 10$ , and the amplitude grows many orders of magnitude in a single betatron period. For example, for  $\tau \sim 3$  ps and  $n_p \sim 10^{18} \text{ cm}^{-3}$ , the fastest growing mode is amplified by seven orders of magnitude in one betatron period. Thus the beam will be disrupted after propagating a short distance, while still in the long-pulse regime. Nonlinear effects may saturate the instability as the beam begins to fill the equilibrium channel, but this would entail at a minimum a large increase in beam emittance.

### C. Discussion of mitigating effects

While a variety of techniques are commonly used to ameliorate beam breakup instabilities, none appears terribly effective for the equilibrium of Fig. 1. In the long-pulse limit, reduction in growth requires a mitigation of the resonance at  $\omega \sim \Omega_p$ , for example, by axial variation of the plasma density. However, this variation must occur on a length scale of order  $L_1$ , which is quite short. In the long-range limit, growth could be controlled by disrupting the resonance at  $k_z = k_\beta$ . This might be accomplished by Landau damping due to a spread in energy within a beam slice [26], energy-sweep damping due to a sweep in energy from head to tail [33], or phase-mix damping due to nonlinear focusing, arising from a radially nonuniform plasma [3]. However, it appears that beam disruption will occur before the beam propagates far enough to reach the long-range regime; thus, these techniques are not relevant except for very short pulses.

We have assumed up to this point that the plasma skin depth  $k_p^{-1}$  is large compared to the channel dimension  $b$  so that the plasma return current may be neglected. For a slab beam this requires  $N_b < (n_p / \pi r_e)^{1/2}$ , where  $N_b = \int n_b dy$  is the beam number density per unit area in the  $x$ - $z$  plane and  $r_e = e^2 / mc^2$  is the classical electron radius. Equivalently, this condition may be written as

$$\frac{I}{I_0} < \frac{1}{\pi} \frac{a_x}{a} \frac{n_p}{n_b}, \quad (28)$$

where  $a_x$  is the beam half-width in  $x$ ,  $I$  is the beam current, and  $I_0 = mc^3 / e \sim 17$  kA. In this limit, the force exerted on the beam by the plasma sheath is essentially a strong “image-displacement” effect [34] and it is appropriate to neglect the plasma return current. If Eq. (28) is not satisfied, the magnetic force on the beam due to the dipole image current will partially cancel the electrostatic force due to the image charge. This will reduce the beam-sheath coupling and, therefore, the instability growth rate.

We conclude that the broad plasma, collisionless equilibrium depicted in Fig. 1 is quite precarious and at best can result in stable propagation only under rather limited circumstances. Next, in Secs. III and IV, we consider modifications to this equilibrium which will tend to reduce growth, namely, a nonuniform plasma (Sec. III) and the effect of plasma-electron collisions (Sec. IV).

### III. TRANSPORT IN A NARROW COLLISIONLESS CHANNEL

In Sec. I and II we considered a beam propagating in a broad, uniform plasma. In such a system, there is no pre-

ferred direction for beam propagation, and perhaps it is not surprising that the beam is subject to a strong instability that disrupts directed transport. In this section we consider a beam guided by a preexisting, narrow underdense plasma channel, surrounded by a broad region of plasma of still lower density. In this situation the beam is focused and guided along the channel axis, and we shall see that the instability can be much weaker.

For definiteness we assume that the ion density takes the form  $n_i = n_p + n_c$ , where  $n_p$  is constant and  $n_c$  is localized within  $|y| < d$ , as depicted in Fig. 5. We also assume  $f = N_c / N_b < 1$ , where  $N_c = \int n_c dy$  is the channel number density per unit area in the  $x$ - $z$  plane. In this case the beam will exclude plasma electrons from a neutralization region  $|y| < b$ , where

$$b = (1 - f) \frac{N_b}{2n_p}. \quad (29)$$

We assume  $b > d$ .

#### A. “Flat-top” channel

We consider first the case in which  $n_c$  is uniform and  $a < d$ , i.e., the channel is “flat-topped” and broader than the beam. In this case, Eqs. (8) and (10) are replaced by

$$\left[ \frac{\partial^2}{\partial \tau^2} + \Omega_p^2(k_x) \right] \eta = \frac{1}{1 - f} \omega_p^2 k_x b e^{-k_x b} \xi, \quad (30)$$

$$\left[ \frac{\partial}{\partial z} \gamma \frac{\partial}{\partial z} + \gamma k_\beta^2 \right] \xi = k_p^2 \eta e^{-k_x b}, \quad (31)$$

with the betatron wave number now determined by the ion density within the channel. Equation (1) is thus replaced by

$$k_\beta = \frac{k_p}{\gamma^{1/2}} R^{1/2}, \quad (32)$$

where  $R = 1 + n_c / n_p$ . Combining Eqs. (30) and (31), the dispersion relation, Eq. (11), is recovered, with Eq. (12) replaced by

$$\Delta^2(\rho) = \frac{1}{R(1 - f)} \frac{2\rho e^{-2\rho}}{1 - e^{-2\rho}}. \quad (33)$$

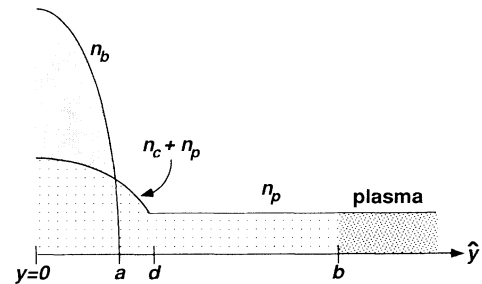


FIG. 5. Finding that propagation in a uniform plasma is highly unstable, we consider a nonuniform plasma with ion density  $n_i = n_p + n_c$ , where  $n_p$  is constant and  $n_c$  is localized within  $|y| < d$ . We will consider the case of a “flat-top” channel (uniform channel density  $n_c$ ) and a “rounded” channel, as depicted here.

For large  $R$ ,  $\Delta^2$  is small and from Eq. (11) one can see that the range of unstable wave numbers is reduced. Identifying the wake amplitude

$$W(k_x) = \frac{1}{1-f} \frac{c^2 k_p^4 k_x b e^{-2k_x b}}{\Omega_p(k_x)}, \quad (34)$$

it is straightforward to show that the asymptotic forms Eqs. (18) and (23) may be taken over directly, with the modified exponents

$$A_1 \approx 0.92 \frac{\Gamma_1^{2/3}}{R^{1/3}(1-f)^{1/3}} (k_\beta z)^{2/3} (\omega_p \tau)^{1/3}, \quad (35)$$

$$A_2 \approx 0.74 \frac{\Gamma_2^{1/3}}{R^{1/3}(1-f)^{1/3}} (k_\beta z)^{1/3} (\omega_p \tau)^{2/3}. \quad (36)$$

Thus for a sufficiently high density ratio ( $R \gg 1$ ), propagation over many betatron wavelengths is feasible. To illustrate this reduction in growth, we consider as an example:  $Rn_p \sim 1 \times 10^{18} \text{ cm}^{-3}$ ,  $\gamma \sim 1 \times 10^5$ ,  $\rho \sim 0.3$ , and  $\tau \sim 3 \text{ ps}$ , corresponding to  $\lambda_\beta \sim 1 \text{ cm}$ . Depicted in Fig. 6 are the numerical solutions for  $|\xi|$ , for several values of  $R$ . Evidently, for large  $R$ , growth is reduced by several orders of magnitude.

In fact, when  $R$  is sufficiently large that  $L_1 > \lambda_\beta$ , a third regime appears in the limit  $\Omega_p \tau \gg 1$ . In this strong-focusing, long-pulse limit [35], the asymptotic form is

$$\xi(z, \tau, k_x) \approx \frac{\tilde{\xi}(k_x)}{2^{3/2} \pi^{1/2}} \frac{A_3^{1/2}}{\Omega_p \tau} e^{A_3} \sin(\Omega_p \tau - k_\beta z), \quad (37)$$

where

$$A_3 = \{\Delta^2(k_\beta z)(\Omega_p \tau)\}^{1/2} \approx 0.59 \frac{\Gamma_1}{R^{1/2}(1-f)^{1/2}} (k_\beta z)^{1/2} (\omega_p \tau)^{1/2}. \quad (38)$$

In terms of a growth length, this is  $A_3 = (z/L_3)^{1/2}$ , where

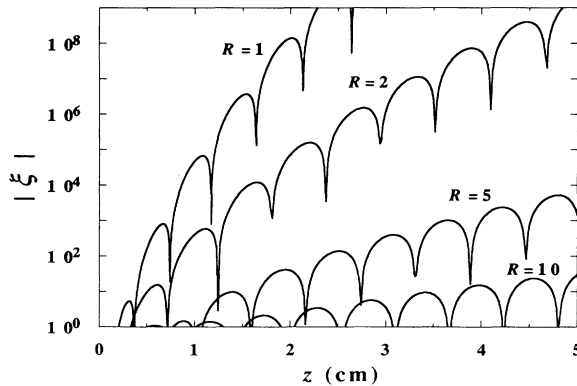


FIG. 6. Depicted is evolution of the amplitude  $|\xi|$  of the beam flute perturbation over five betatron wavelengths as computed numerically from Eqs. (30) and (31). The amplitude is evaluated at the pulse tail for  $R=1, 5, 10$ , and  $20$ . Other parameters are  $Rn_p \sim 1 \times 10^{18} \text{ cm}^{-3}$ ,  $\gamma \sim 1 \times 10^5$ ,  $k_x b \sim 0.3$ ,  $T=3 \text{ ps}$ , and  $\lambda_\beta \sim 1.06 \text{ cm}$ . Without some channel enhancement (i.e., for  $R=1$ ), the system is disastrously unstable.

$$L_3 = \frac{\gamma k_\beta}{W(k_x) \tau} \approx 0.45 \frac{\lambda_\beta}{\omega_p \tau} \frac{R(1-f)}{\Gamma_1^2(k_x b)}. \quad (39)$$

However, in this limit, where the growth length is longer than the betatron period, phase mixing due to a spread in betatron frequency can damp growth significantly, as we show next.

### B. Distributed betatron resonance

If the beam is not monoenergetic, or if the focusing force is nonlinear (e.g., in an ion channel with a rounded density profile), there will be a distribution in betatron wave numbers. In the strong-focusing limit this will spread the betatron resonance and lead to a significant reduction in growth. The instability is then convective, rather than absolute; this is the result of “phase mixing” which converts the coherent flute energy into thermal energy (beam emittance growth).

We will model this effect by representing a beam slice as a superposition of macroparticles [36] with displacement  $\xi(z, \tau, k_x; \Omega_\beta)$  and some distribution  $g(\Omega_\beta)$  in betatron wave number  $\Omega_\beta$  [37]. The mean beam displacement is given by

$$\bar{\xi}(z, \tau, k_x) = \int d\Omega_\beta g(\Omega_\beta) \xi(z, \tau, k_x; \Omega_\beta), \quad (40)$$

where the normalization condition  $\int d\Omega_\beta g(\Omega_\beta) = 1$  is assumed. Equations (30) and (31) are replaced by

$$\left[ \frac{\partial^2}{\partial \tau^2} + \Omega_p^2(k_x) \right] \eta(z, \tau, k_x) = \frac{1}{1-f} \omega_p^2 k_x b e^{-k_x b} \bar{\xi}(z, \tau, k_x), \quad (41)$$

$$\left[ \frac{\partial}{\partial z} \gamma \frac{\partial}{\partial z} + \gamma \Omega_\beta^2 \right] \xi(z, \tau, k_x; \Omega_\beta) = k_p^2 e^{-k_x b} \eta(z, \tau, k_x). \quad (42)$$

The dispersion relation is obtained by combining Eqs. (40)–(42):

$$1 - \frac{\omega^2}{\Omega_p^2} = \Delta^2 k_\beta^2 \int d\Omega_\beta \frac{g(\Omega_\beta)}{\Omega_\beta^2 - k_z^2} \equiv \Lambda_r + i\Lambda_i, \quad (43)$$

where  $\Lambda_r$  and  $\Lambda_i$  are functions of  $k_x$  (through  $\Delta^2$ ) and  $k_z$ :

$$\Lambda_r = \Delta^2 k_\beta^2 \left[ \int d\Omega_\beta \frac{g(\Omega_\beta) - g(k_z)}{\Omega_\beta^2 - k_z^2} + \frac{g(k_z)}{2k_z} \ln \left| \frac{\Omega_+ - k_z}{\Omega_- - k_z} \frac{\Omega_- + k_z}{\Omega_+ + k_z} \right| \right], \quad (44)$$

$$\Lambda_i = \frac{\pi \Delta^2 k_\beta^2}{2k_z} g(k_z). \quad (45)$$

Here,  $g$  is assumed to vanish outside a finite interval  $[\Omega_-, \Omega_+]$ , where  $\Omega_+ = k_\beta$  with  $k_\beta$  given by Eq. (32). Note that the integral is continued from the upper  $k_z$  plane, as is appropriate for the initial-value problem [38,39]. The lower limit is  $\Omega_- = k_\beta(1-\delta)$ , where  $\delta$  is the

fractional width of the distribution.

Up to the quadrature of Eq. (43), the solutions of the dispersion relation are then determined as functions of real  $k_z$  and  $k_x$ , through  $\Lambda_r$  and  $\Lambda_i$  as follows:

$$\frac{\omega}{\Omega_p} = \pm \begin{cases} \{1 - \Lambda_r\}^{1/2}, & \Lambda_i = 0, \Lambda_r < 1 \\ i\{\Lambda_r - 1\}^{1/2}, & \Lambda_i = 0, \Lambda_r > 1 \end{cases} \quad (46)$$

and for  $\Lambda_i \neq 0$ .

$$\text{Re} \left[ \frac{\omega}{\Omega_p} \right] = \pm \frac{1}{2^{1/2}} \{1 - \Lambda_r + [(1 - \Lambda_r)^2 + \Lambda_i^2]^{1/2}\}^{1/2}, \quad (47)$$

$$\text{Im} \left[ \frac{\omega}{\Omega_p} \right] = \mp \frac{\Lambda_i}{2^{1/2}} \{1 - \Lambda_r + [(1 - \Lambda_r)^2 + \Lambda_i^2]^{1/2}\}^{-1/2}. \quad (48)$$

To make this more quantitative, we consider two specific examples. The simplest example is a “flat” distribution,

$$g(\Omega_\beta) = \frac{1}{\delta k_\beta} H(\Omega_+ - \Omega_\beta) H(\Omega_\beta - \Omega_-), \quad (49)$$

for which the dispersion integral is

$$\Lambda_r + i\Lambda_i = \frac{\Delta^2}{2\delta} \frac{k_\beta}{k_z} \left\{ \ln \left| \frac{\Omega_+ - k_z}{k_z - \Omega_-} \frac{\Omega_- + k_z}{\Omega_+ + k_z} \right| + i\pi H(\Omega_-^2 < k_z^2 < \Omega_+^2) \right\}. \quad (50)$$

For illustration, solutions for  $\omega$  as a function of real  $k_z$  are depicted in Fig. 7 for several values of  $R$ , with  $k_x b = 0.3$ ,  $f \ll 1$ , and  $a = d$ . Analysis of the dispersion relation as detailed in the Appendix shows that for  $\delta \gg \Delta^2$  the length for saturation is

$$L_{\text{sat}} = \frac{1}{2\pi} \Omega_p \tau \frac{\Delta^2}{\delta^2} \lambda_\beta, \quad (51)$$

and the amplitude at saturation is

$$\xi_{\text{sat}} \approx 0.8 \frac{\Delta^2}{\delta^{5/3} A_{\text{sat}}^{1/3}} \exp(A_{\text{sat}}), \quad (52)$$

with exponent

$$A_{\text{sat}} = \frac{\pi}{4} \Omega_p \tau \frac{\Delta^2}{\delta}. \quad (53)$$

Depicted in Fig. 8 are the solutions for  $\bar{\xi}$ , for several values of  $R$ , with  $\delta = 5\%$ , for illustration.

As a second example, we consider the distribution in betatron frequency resulting from a parabolic ion profile:

$$n_i = n_p + n_c(0) \left( 1 - \frac{y^2}{d^2} \right) H(d - y), \quad (54)$$

and we assume  $d \geq a$  (as in Fig. 5), so that no beam electrons oscillate beyond the parabolic channel. The equilibrium transverse motion of a beam electron is then a periodic oscillation in the nonlinear pinch potential,

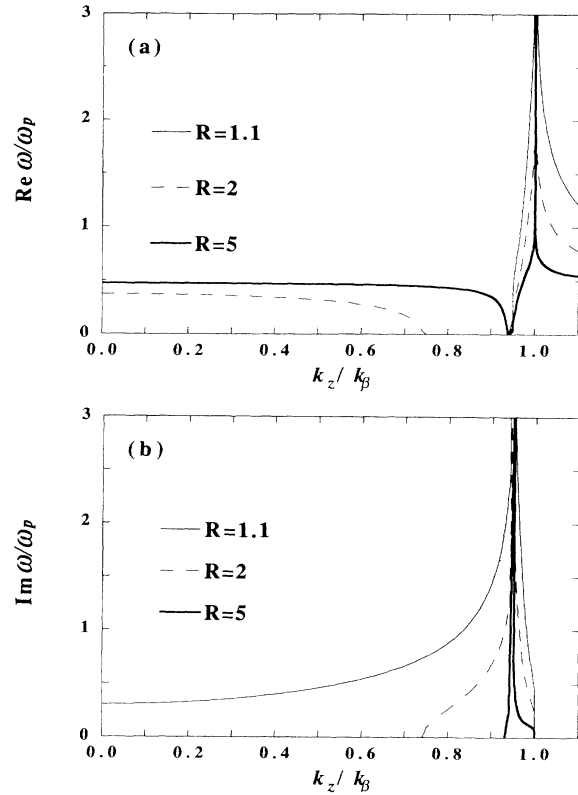


FIG. 7. For illustration, several solutions of the dispersion relation, Eqs. (43) and (50), are depicted for a flat distribution in  $\Omega_\beta$  with a spread in a betatron period of  $\delta = 5\%$ : (a)  $\text{Re}(\omega)$  and (b)  $\text{Im}(\omega)$  are evaluated for  $R = 1.1, 2$ , and  $5$ , with  $f \ll 1$  and  $k_x b \sim 0.3$ . The normalization is the angular plasma frequency  $\omega_p$ .

$$\psi = \frac{mc^2}{2e} R k_p^2 \left\{ y^2 - \frac{y^4}{\hat{d}^2} \right\}, \quad (55)$$

where

$$\hat{d} = 6^{1/2} \left[ 1 - \frac{1}{R} \right]^{-1/2} d \quad (56)$$

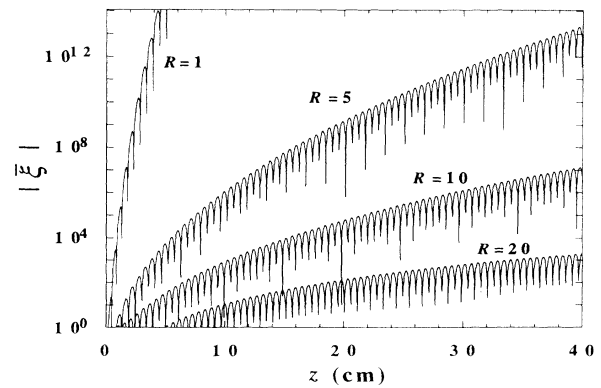


FIG. 8. Depicted is the evolution of the amplitude  $|\bar{\xi}|$  of the beam flute perturbation over 40 betatron wavelengths, as computed numerically from Eqs. (41) and (42), for a uniform distribution in betatron frequency of width  $\delta = 5\%$ , i.e.,  $0.95k_\beta < \Omega_\beta < k_\beta$ . The amplitude is evaluated at the pulse tail for  $R = 1, 5, 10$ , and  $20$ . Other parameters are as in Fig. 6.

is a length characterizing the degree of nonlinearity and  $R = 1 + n_c(0)/n_p$ . For  $R \rightarrow 1$  (vanishingly weak localized channel),  $\hat{d} \rightarrow \infty$  and the potential reduces to a simple harmonic-oscillator well. For finite  $\hat{d}$ , the betatron motion is anharmonic, with a period  $2\pi/\Omega_\beta$ , depending on the amplitude  $y_m$  and given by

$$\frac{\Omega_\beta(y_m)}{\Omega_\beta(0)} = \frac{\pi}{2} \left\{ 1 - \left[ \frac{y_m}{\hat{d}} \right]^2 \right\}^{1/2} \left[ K \left[ \frac{y_m}{(\hat{d}^2 - y_m^2)^{1/2}} \right] \right]^{-1} \approx \left\{ 1 - \frac{3}{2} \left[ \frac{y_m}{\hat{d}} \right]^2 \right\}^{1/2}, \quad (57)$$

where  $\Omega_\beta(0) = \Omega_+ = k_\beta$ , as given by Eq. (32), and  $K$  is the complete elliptic integral of the first kind [40]. The dependence of  $\Omega_\beta$  on  $y_m$  is well fit by the approximate form on the right of Eq. (57), as shown in Fig. 9 [41]. In this model the frequency spread  $\delta = (\Omega_+ - \Omega_-)/\Omega_+$  is

$$\delta = 1 - \left\{ 1 - \frac{1}{4} \left[ \frac{a}{\hat{d}} \right]^2 \left[ 1 - \frac{1}{R} \right] \right\}^{1/2}, \quad (58)$$

obtained by combining Eqs. (56) and (57). Note that for  $a = d$  and  $R \rightarrow \infty$ ,  $\delta \sim 13\%$ , the maximum frequency spread in this model (a consequence of assuming  $a \leq d$ ).

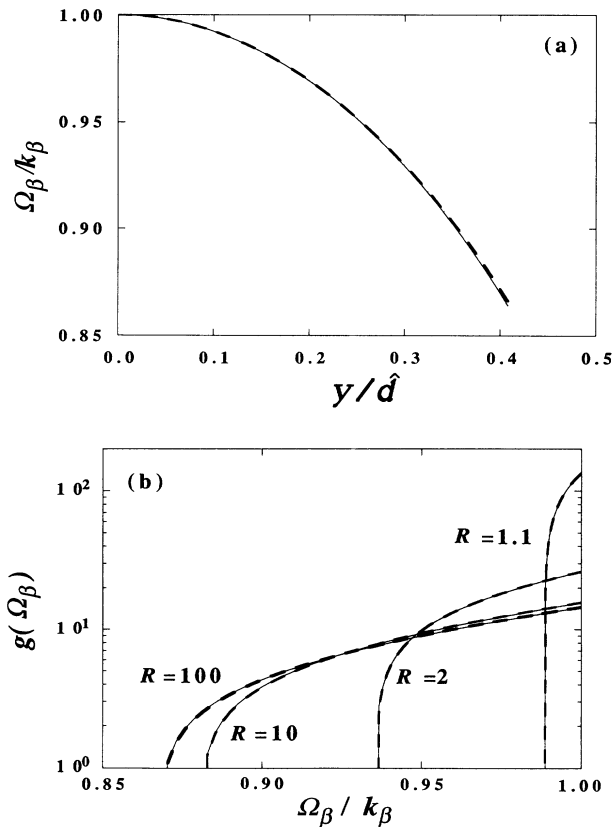


FIG. 9. (a) For the rounded channel of Eq. (54), the betatron frequency  $\Omega_\beta$  as given by Eq. (62) is a function of the betatron amplitude  $y_m$  normalized by  $\hat{d}$  as given by Eq. (56). (b) Depicted is the distribution in betatron frequency, from Eq. (61), for various values of the channel density ratio  $R$ , with the exact results from Eq. (59) overlayed (they are indistinguishable).

The distribution  $g(\Omega_\beta)$  is determined by the distribution  $F$  in transverse energy  $H_\perp = \psi(y_m)$ , according to

$$g(\Omega_\beta) = F(H_\perp) \left| \frac{d\Omega_\beta}{dH_\perp} \right|^{-1}. \quad (59)$$

As an example, we consider  $F(H_\perp) \propto \sqrt{T_\perp - H_\perp}$ , where  $T_\perp = \psi(a)$  is a constant proportional to the beam temperature (or emittance). The beam profile is then

$$n_b(y) = n_b(0) \left\{ 1 - \frac{y^2}{a^2} \right\} \left\{ 1 - \frac{y^2}{\hat{d}^2 - a^2} \right\}. \quad (60)$$

Since  $\hat{d}^2 \geq 6a^2$ , this is very nearly a parabolic profile (exactly so for linear focusing). For this model beam distribution,  $g$  is well fit by

$$g(\Omega_\beta) \approx g_0 \Omega_\beta (\Omega_\beta^2 - \frac{2}{3} \Omega_+^2) (\Omega_\beta^2 - \Omega_-^2)^{1/2}, \quad (61)$$

where the normalization constant is

$$g_0^{-1} = \frac{1}{15} (\Omega_+^2 - \Omega_-^2)^{3/2} (\Omega_+^2 + 2\Omega_-^2). \quad (62)$$

This distribution is depicted in Fig. 9 for several values of  $R$ .

Combining Eqs. (44), (45), and (61), the quantities  $\Lambda_r$  and  $\Lambda_i$  (and hence the dispersion relation) may be expressed in terms of the variables  $Q = (\Omega_+^2 - \Omega_-^2)^{1/2}$ ,  $K = |\Omega_-^2 - k_z^2|^{1/2}$ , and the integral

$$\vartheta(k_z^2) = \begin{cases} Q - K \tan^{-1} \left[ \frac{Q}{K} \right], & k_z^2 < \Omega_-^2 \\ Q + \frac{1}{2} K \left[ i\pi + \ln \left[ \frac{Q-K}{Q+K} \right] \right], & \Omega_-^2 < k_z^2 < \Omega_+^2 \\ Q + \frac{1}{2} K \ln \left[ \frac{K-Q}{K+Q} \right], & \Omega_+^2 < k_z^2 \end{cases} \quad (63)$$

as

$$\Lambda_r + i\Lambda_i = g_0 \Delta^2 k_\beta^2 \{ (k_z^2 - \frac{2}{3} \Omega_+^2) \vartheta(k_z^2) + \frac{1}{3} Q^3 \}. \quad (64)$$

For illustration, solutions for  $\omega$  as a function of real  $k_z$  are depicted in Fig. 10 for several values of  $R$ , with  $k_x b \sim 0.3$ ,  $f \ll 1$ , and  $a = d$ . The analysis given in the Appendix provides an estimate of the length scale for saturation, in the limit  $\delta \gg \Delta^2$ :

$$L_{\text{sat}} = \frac{1}{\pi} \Omega_p \tau \frac{\Delta^2}{\delta^2} \lambda_\beta. \quad (65)$$

The amplitude at saturation is roughly

$$\xi_{\text{sat}} \approx 0.2 \frac{\Delta^2}{\delta A_{\text{sat}}^{1/2}} \exp(A_{\text{sat}}), \quad (66)$$

with exponent

$$A_{\text{sat}} = \omega_m \tau \approx \Omega_p \tau \frac{\Delta^2}{\delta}, \quad (67)$$

where  $\omega_m$  is the maximum of  $\text{Im}(\omega)$  on the real  $k_z$  axis

and is given approximately by the expression on the right. Examples of evolution of the flute instability computed numerically with this distribution are depicted in Fig. 11.

From the work of this section one can see that growth may be considerably reduced for an enhanced ion profile due to the stronger focusing and effectively lower wake frequency. With a spread in betatron frequency, and large  $R$ , the system quickly saturates due to phase mixing. Evidently, the scalings for saturation length and amplitude are not very sensitive to the form of the distribution, as one can see by comparing Eqs. (51)–(53) with Eqs. (65)–(67). In particular, the logarithmic divergence in the dispersion relation for the flat distribution is not inconsistent with a convective solution.

While we have considered only the case in which the plasma is preformed the situation will be similar if the beam propagates along a plasma channel formed by rapid ionization at the beam head. Depending on the dominant ionization process [42] (collisional, avalanche, tunneling, or stripping), one could expect a profile similar to that of Eq. (60), with comparable beam and channel waists,  $a \sim d$ . Moreover, if any initial ionization is small, then  $R \gg 1$ , and one may expect significant nonlinearity and damping.

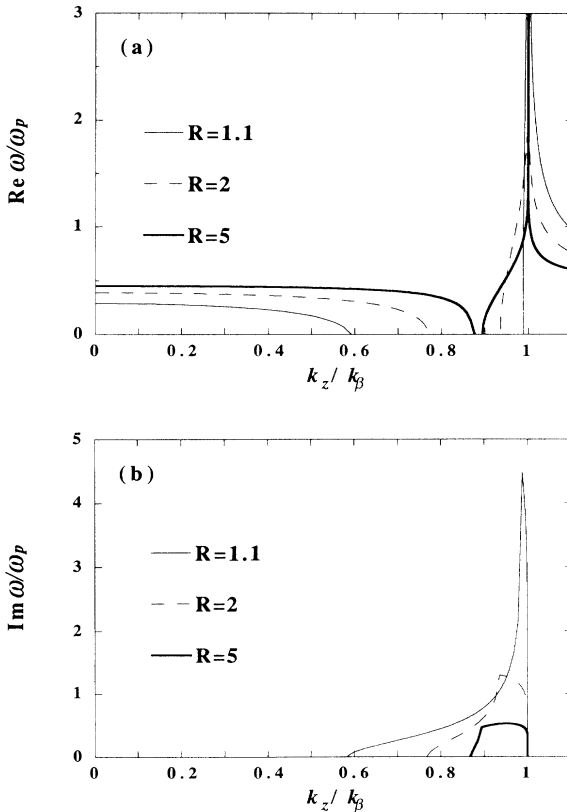


FIG. 10. Several solutions of the dispersion relation, Eqs. (43) and (64), for (a)  $\text{Re}(\omega)$  and (b)  $\text{Im}(\omega)$  are depicted for  $R = 1.1, 2$ , and  $5$ , with  $f \ll 1$  and  $k_x b \sim 0.3$ , with normalization  $\omega_p$ , the angular plasma frequency. The distribution in  $\Omega_\beta$  is that of a beam in a parabolic channel, as in Eq. (61).

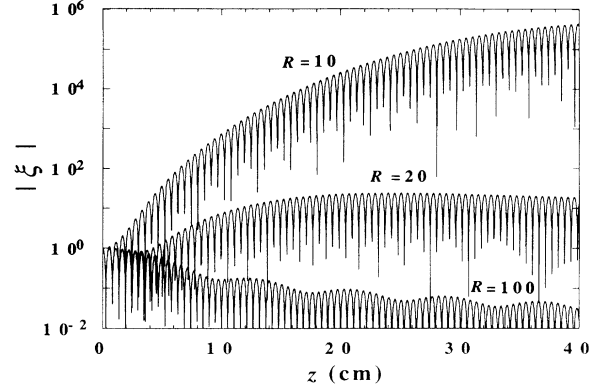


FIG. 11. Depicted is the evolution of the amplitude  $|\bar{\xi}|$  of the beam flute perturbation over 40 betatron wavelengths, as computed numerically from Eqs. (41) and (42), for the distribution in betatron frequency of Eq. (61) corresponding to a parabolic channel. The amplitude is evaluated at the pulse tail for  $R = 10, 20$ , and  $100$ , corresponding to  $\delta = 11.9\%$ ,  $12.6\%$ , and  $13.1\%$ . Other parameters are as in Fig. 6.

#### IV. TRANSPORT IN A NARROW COLLISIONAL CHANNEL

Up to now, we have considered a collisionless plasma. In this section we consider the effect on beam propagation of plasma-electron collisions. We will model collisions phenomenologically, adopting a constant collision rate of plasma electrons with ions and neutrals,  $\nu$ , and modifying Eq. (5) to read

$$\frac{\partial \mathbf{V}_e}{\partial t} \approx \frac{e}{m} \nabla_1 \phi - \nu \mathbf{V}_e. \quad (68)$$

The resulting flute equations are just Eq. (41) modified with the addition of a damping term,

$$\left[ \frac{\partial^2}{\partial \tau^2} + \nu \frac{\partial}{\partial \tau} \Omega_p^2(k_x) \right] \eta(z, \tau, k_x) = \frac{1}{1-f} \omega_p^2 k_x b e^{-k_x b} \bar{\xi}(z, \tau, k_x). \quad (69)$$

and Eq. (42), unchanged. The wake may take different forms depending on whether the flute oscillations are underdamped, critically damped, or overdamped. The wake is overdamped for modes such that  $\nu > 2\Omega_p$ ; in terms of flute wave number, this condition is [43]

$$k_x b < -\frac{1}{2} \ln \left[ 1 - \frac{\nu^2}{2\omega_p^2} \right] \approx \left[ \frac{\nu}{2\omega_p} \right]^2. \quad (70)$$

Typically, one expects such long flute wavelengths to be far from those giving maximum growth, and we thus neglect the overdamped and critically damped cases.

In the underdamped case,  $\nu < 2\Omega_p$ , and the wake takes the form

$$W(k_x, \tau) = W(k_x) \sin[\hat{\Omega}_p(k_x) \tau] \exp[-\frac{1}{2} \nu \tau], \quad (71)$$

with amplitude

$$W(k_x) = \frac{1}{1-f} \frac{c^2 k_p^4 k_x b e^{-2k_x b}}{\hat{\Omega}_p(k_x)} \quad (72)$$

and resonant frequency lowered due to damping,

$$\hat{\Omega}_p(k_x) = [\Omega_p^2(k_x) - \frac{1}{4}\nu^2]^{1/2}. \quad (73)$$

Physically, one expects collisions to convert the energy of the coherent flute motion to thermal energy of the plasma. This damping is exponential in  $\tau$ , while the instability growth is less than exponential. Consequently, at a point  $z$  along the beamline and after some point  $\tau_p(z)$  along an infinite beam, the flute amplitude will diminish as a function of  $\tau$ . The peak in growth will convect backward along the beam. For this to be observable in a finite beam, the pulse length must be sufficiently long that  $\nu T \sim A$ , where  $A$  is the number of exponentiations in the absence of collisions. In this case, far enough from the beam head, such that  $\hat{\Omega}_p \tau \gg 1$ , there are two regimes of asymptotic growth, corresponding to weak and strong focusing. When focusing is weak, the convecting peak in growth occurs at

$$\tau_p = \frac{3^{9/4}}{2^{9/4}} \frac{\Gamma_1}{R^{1/2}(1-f)^{1/2}} \frac{\omega_p^{1/2}}{\nu^{3/2}} (k_\beta z), \quad (74)$$

where  $\tau_p < T$  is assumed. The peak amplitude varies as  $\exp(z/L'_1)$ , where

$$L'_1 \approx \frac{2^{5/4}}{3^{3/4}\pi} \frac{R^{1/2}(1-f)^{1/2}}{\Gamma_1} \left[ \frac{\nu}{\omega_p} \right]^{1/2} \lambda_\beta. \quad (75)$$

When focusing is strong, the convecting peak in growth occurs at

$$\tau_p = \frac{1}{2^{3/2}} \frac{\Gamma_1^2}{R(1-f)} \frac{\omega_p}{\nu^2} (k_\beta z), \quad (76)$$

and the peak amplitude varies as  $\exp(z/L'_3)$ , where

$$L'_3 \approx \frac{2^{3/2}}{\pi} \frac{R(1-f)}{\Gamma_1^2} \frac{\nu}{\omega_p} \lambda_\beta. \quad (77)$$

Note that with a distribution in betatron period and collisions, the instability can in principle be stabilized [44]. This is seen by analyzing the dispersion relation, Eq. (43), modified by collisions

$$1 - i \frac{\nu \omega}{\Omega_p^2} - \frac{\omega^2}{\Omega_p^2} = \Lambda_r + i \Lambda_i. \quad (78)$$

Defining the normalized collision rate  $\tilde{\nu} \equiv \nu/\Omega_p$ , the solution of the dispersion relation is determined as follows:

$$\frac{\omega}{\Omega_p} = \pm \begin{cases} \pm \{1 - \frac{1}{4}\tilde{\nu}^2 - \Lambda_r\}^{1/2} - i \frac{\tilde{\nu}}{2} \Lambda_i = 0, & \Lambda_r < 1 - \frac{1}{4}\tilde{\nu}^2 \\ \pm i \{\Lambda_r - 1 + \frac{1}{4}\tilde{\nu}^2\}^{1/2}, & \Lambda_i = 0, \Lambda_r > 1 - \frac{1}{4}\tilde{\nu}^2 \end{cases} \quad (79)$$

and for  $\Lambda_i \neq 0$ ,

$$\text{Re} \left[ \frac{\omega}{\Omega_p} \right] = \pm \frac{1}{2^{1/2}} \{1 - \frac{1}{4}\tilde{\nu}^2 - \Lambda_r + [(1 - \frac{1}{4}\tilde{\nu}^2 - \Lambda_r)^2 + \Lambda_i^2]^{1/2}\}^{1/2}, \quad (80)$$

$$\text{Im} \left[ \frac{\omega}{\Omega_p} \right] = -\frac{\tilde{\nu}}{2} \mp \frac{\Lambda_i}{2^{1/2}} \{1 - \frac{1}{4}\tilde{\nu}^2 - \Lambda_r + [(1 - \frac{1}{4}\tilde{\nu}^2 - \Lambda_r)^2 + \Lambda_i^2]^{1/2}\}^{-1/2}. \quad (81)$$

The condition for stability is that  $\omega$  be real along the entire  $k_z$  axis. A bit of algebra reduces this condition to

$$\tilde{\nu} > \max_{k_z} \left[ \frac{\Lambda_i}{\{1 - \Lambda_r\}^{1/2}} \right], \quad (82)$$

$$\max_{k_z} (\Lambda_r) < 1 - \frac{1}{4}\tilde{\nu}^2. \quad (83)$$

For the parabolic distribution of Eq. (61), with  $a = d$  and  $\rho = 0.3$ , numerical solution of Eqs. (80) and (81) shows that this requires roughly  $\nu/\omega_p \geq 8/R$  and  $R > 10$ . Thus, for large  $R$  and a significant  $\nu/\omega_p$ , the combination of betatron distribution and collisions can stabilize the system. This is illustrated in Fig. 12 for several values  $\nu/\omega_p$  and  $R$ , with a parabolic channel distribution in betatron frequency as in Eq. (61). It should be added that when the collision rate is appreciable, one should also consider a possible resistive flute instability at the beam head (i.e.,

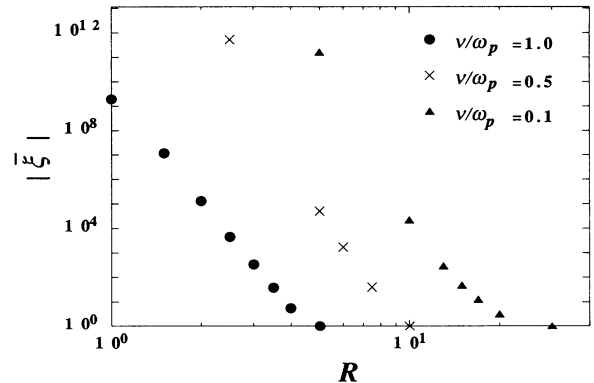


FIG. 12. To illustrate the combined effect of collisions and a distribution in betatron period, the maximum in amplitude (over  $\tau$  and  $z$ ) after 40 betatron periods is depicted for various values of  $\nu/\omega_p$  and  $R$ , with a distribution as for a parabolic channel. Other parameters are as in Fig. 6.

the slab-beam analog of the “resistive-hose” instability [36]).

## V. CONCLUSIONS

We have studied a transverse flute instability arising from an electrostatic resonance of a relativistic slab electron beam in a collisionless underdense plasma, with negligible return current. It is instructive to contrast this mechanism with other well-known transverse instabilities of a beam-plasma system. For example, the resistive-hose instability [36,45,46] arises due to dissipation of eddy currents in a highly collisional overdense plasma. In this case, nonlinear focusing and the resulting distribution in betatron period are *intrinsic* features of the self-pinch equilibrium. This is to be contrasted with the ion-focused regime considered in this paper, wherein nonlinear focusing of the beam occurs only if the radial ion-density profile is nonuniform. There is a second well-known electrostatic instability of the ion-focused regime, the ion-hose instability [2]. For the ion hose instability the focusing force on individual ions in the beam fields is intrinsically nonlinear, and this results in a spread in resonant wake or “ion-slosh” frequencies, formally akin to “stagger tuning” [30]. In addition, the ion molecular weight is a free parameter which may be chosen quite large, thereby reducing the resonant wake frequency and bringing the beam into the short-pulse regime of beam breakup growth.

The electron-coupled flute instability in a broad plasma is then distinguished from these other transverse instabilities by the paucity of adjustable parameters, the coherence of the plasma response, and the absence of *intrinsic* nonlinearity in the beam motion. This instability renders impractical the ion-focused propagation of a slab beam in a broad *uniform* plasma in the large skin-depth limit.

However, when the ion profile is significantly peaked on axis, focusing is stronger and propagation to a longer range is feasible. If in addition, the ion-channel profile is rounded and narrow, falling off within the beam volume, the resulting spread in betatron frequency introduces phase-mix damping. The instability is then convective, and propagation to arbitrarily long range becomes possible if the beam duration is short enough. It should be added that for some applications (e.g., a continuous plasma focus) it remains unclear to what extent one could insure a rounded channel and nonlinear focusing, and whether the focus would still be useful in this case.

We have also shown that damping due to plasma-electron collisions will reduce growth. A combination of a distribution in betatron frequencies and plasma-electron collisions can in principle stabilize the instability if the channel enhancement and the collision rate are appreciable.

This work underscores the importance of a thorough study of beam and secondary ionization profiles for parameters typical of high-energy applications. In addition, the effect of return current in the small-skin-depth limit merits much further attention.

## ACKNOWLEDGMENTS

Work in Japan was supported by the National Laboratory for High Energy Physics (KEK), the Japan Society for the Promotion of Science, and the U.S. National Science Foundation. Work at NRL was supported by DARPA and monitored by the Naval Surface Weapons Center (NSWC) under ARPA Order 7781. Work at LLNL was supported by DOE Contract No. W-7405-ENG-48 and by the Department of Defense under SDIO/SDC-ATC MIPR No. W31RPD-7-D4041. Work was also performed at Lawrence Berkeley Laboratory under DOE Contract No. DE-AC03-76SF00098.

## APPENDIX: ASYMPTOTIC BEAM BREAKUP GROWTH

The asymptotic growth of two-stream and beam breakup instabilities is the subject of a vast literature. The problem was first studied in connection with the longitudinal two-stream instability by Buneman [22], Briggs [23,24], and Bers [25]. Subsequently, and independently, the problem was examined by Panofsky and Bander [47] in connection with transverse stability in the Stanford Linear Collider (SLC). Further work on beam breakup was performed by Chao, Richter, and Yao [31], again for application to the SLC, and by Neil, Hall, and Cooper [35,44] for application to induction accelerators. A review of this work from the beam breakup or accelerator physics point of view has been given by Lau [30]. A number of review articles on “the” beam-plasma interaction have been written over the decades [48]. In this appendix we review briefly the relevant steepest-descent calculations and go on to confirm the accuracy of the analytic forms by comparison with more exact numerical solutions. We then proceed to derive expressions for asymptotic saturation in the presence of the flat and parabolic betatron distributions. These last calculations bear comparison to recent work by Takayama [49] for the case of beam breakup in a structure with “linear detuning.”

Consider the beam breakup equation with uniform focusing and no acceleration,

$$\left[ \frac{\partial}{\partial z} \gamma \frac{\partial}{\partial z} + \gamma k_\beta^2 \right] \xi(z, \tau) = \int_0^\tau ds' W(\tau - \tau') \xi(z, \tau'), \quad (\text{A1})$$

and initial conditions  $\xi(z, \tau) = H(\tau)$ . The solution up to quadrature is given by the inverse Laplace transform

$$\xi(z, \tau) = \frac{1}{2\pi i} \int_{-i\infty+0^+}^{+i\infty+0^+} dp \frac{1}{p} \exp(p\tau) \times \cos \left\{ k_\beta z \left[ 1 - \frac{\tilde{W}(p)}{\gamma k_\beta^2} \right]^{1/2} \right\}, \quad (\text{A2})$$

where  $\tilde{W}(p)$  is the Laplace transform of  $W(\tau)$  and is, in general, analytic in the right half-plane. It is convenient to write this as  $\xi = (\xi_+ + \xi_-)/2$ , where

$$\xi_\sigma(z, \tau) = \frac{1}{2\pi i} \int_{-i\infty+0^+}^{+i\infty+0^+} dp \frac{1}{p} \exp\{\varphi_\sigma(z, \tau, p)\}, \quad (\text{A3})$$

with  $\sigma = \pm 1$  and

$$\varphi_\sigma(z, \tau, p) = p\tau + i\sigma k_\beta z \left[ 1 - \frac{\tilde{W}(p)}{\gamma k_\beta^2} \right]^{1/2}. \quad (\text{A4})$$

From the stationary points  $p_{s\sigma}$  such that  $\partial\varphi_\sigma/\partial p \sim 0$ , one determines the asymptotic growth using the method of steepest descents. When at most one stationary point yields growth and provided  $\varphi^{(2)} \neq 0$ , the asymptotic form is

$$\xi_\sigma(z, \tau) \approx \frac{1}{(2\pi\varphi_\sigma^{(2)})^{1/2}} \frac{1}{p_{s\sigma}} \exp(\varphi_\sigma). \quad (\text{A5})$$

Here,  $\varphi^{(2)}$  is the second derivative with respect to  $p$  and all quantities in Eq. (A5) are evaluated at  $p_{s\sigma}$ .

We will consider first a damped sinusoidal wake,

$$W(\tau) = W_0 \sin(\Omega_p \tau) \exp(-\frac{1}{2}\nu\tau), \quad (\text{A6})$$

for which the Laplace transform is

$$W(p) = W_0 \frac{\Omega_p}{p^2 + \nu p + \Omega_p^2}. \quad (\text{A7})$$

Then,

$$\varphi_\sigma(z, \tau, p) = p\tau + i\sigma k_\beta z \left[ 1 - \frac{W_0}{\gamma k_\beta^2} \frac{\Omega_p}{p^2 + \nu p + \Omega_p^2} \right]^{1/2}. \quad (\text{A8})$$

To determine the stationary points in general requires the solution of an eighth-order polynomial in  $p$ . In various limits, however, these points are quite easily determined, and the results are quite accurate within their range of validity. We consider each regime in turn.

In the short-pulse (“head-tail”) regime, where  $\Omega_p \tau$  is small, it is reasonable to neglect the poles in Eq. (A8), in effect replacing the sinusoidal wake with a linear wake. In this limit, we have

$$\varphi_\sigma(z, \tau, p) \approx p\tau + i\sigma k_\beta z \left[ 1 - \frac{W_0}{\gamma k_\beta^2} \frac{\Omega_p}{p^2} \right]^{1/2}. \quad (\text{A9})$$

Within this regime we may distinguish the weak-focusing limit (Panofsky and Bander [47]) and the strong-focusing limit (Chao, Richter, and Yao [31]). In the weak-focusing limit, the influence of the wake is much larger than that of the focusing fields, and

$$\varphi_\sigma(z, \tau, p) \approx p\tau + i\sigma z \left[ -\frac{W_0 \Omega_p}{\gamma} \right]^{1/2} \frac{1}{p}. \quad (\text{A10})$$

The only stationary point exhibiting growth is

$$p_{+s} = \left[ \frac{z^2}{\tau^2} \frac{W_0 \Omega_p}{\gamma} \right]^{1/4}, \quad (\text{A11})$$

and carrying through Eq. (A5), the asymptotic form is

$$\xi(z, s) \approx \frac{1}{\sqrt{8\pi A}} e^A, \quad (\text{A12})$$

where the exponent

$$A = 2(\tau z)^{1/2} \left[ \frac{W_0 \Omega_p}{\gamma} \right]^{1/4}. \quad (\text{A13})$$

Comparison of this form with a numerical example is exhibited in Fig. 13. The pulse should be short in the sense that  $A \gg \Omega_p \tau$ , and the focusing should be weak in the sense that  $A \gg k_\beta z$ .

In the strong-focusing limit, the influence of the wake is quite weak, and

$$\varphi_\sigma(z, \tau, p) \approx p\tau + i\sigma k_\beta z \left[ 1 - \frac{W_0 \Omega_p}{2\gamma k_\beta^2} \frac{1}{p^2} \right]. \quad (\text{A14})$$

The stationary points are

$$p_{s\sigma} = \left[ \frac{W_0 \Omega_p z}{\gamma k_\beta \tau} \right]^{1/3} \exp(-i\pi\sigma/6). \quad (\text{A15})$$

And applying Eq. (A5), the solution obtained is just that of Eq. (23). Comparison of this form with a numerical example is exhibited in Fig. 14.

Next consider the long-pulse limit, which is the subject of Sec. II B of the main text. In this limit, one expects a dominant contribution near one of the poles of Eq. (A8). In the strong-focusing limit, expanding the square root, the stationary points are

$$p_\sigma = -i\sigma \Omega_p - \frac{1}{2}\nu + \left[ \frac{z W_0}{\gamma k_\beta \tau} \right]^{1/2}. \quad (\text{A16})$$

The solution takes the form

$$\begin{aligned} \xi(z, \tau) \approx & \frac{1}{2^{3/2} \pi^{1/2}} \frac{A^{1/2}}{\Omega_p \tau} \exp(A - \frac{1}{2}\nu\tau) \\ & \times \{ \sin(k_\beta z - \Omega_p \tau) - \frac{\nu}{2\Omega_p} \cos(k_\beta z - \Omega_p \tau) \}, \end{aligned} \quad (\text{A17})$$

with the exponent

$$A = \left[ \frac{z \tau W_0}{\gamma k_\beta} \right]^{1/2}. \quad (\text{A18})$$

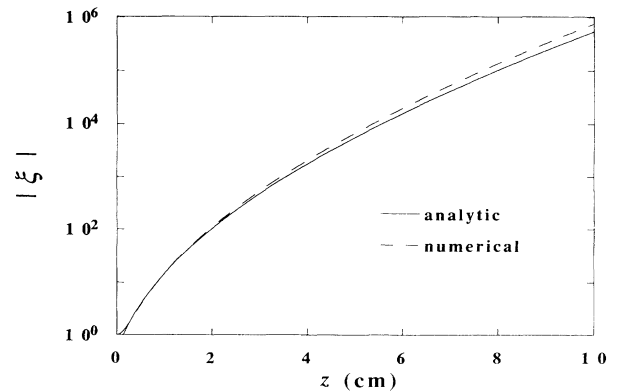


FIG. 13. Comparison of the weak-focusing, short-pulse asymptotic form of Eq. (A12) with the numerical solution for  $Rn_p \sim 1 \times 10^{18} \text{ cm}^{-3}$ ,  $\gamma \sim 1 \times 10^5$ ,  $k_x b \sim 0.3$ ,  $T = 0.05 \text{ ps}$ ,  $R = 1$ , and  $k_\beta = 0$ .

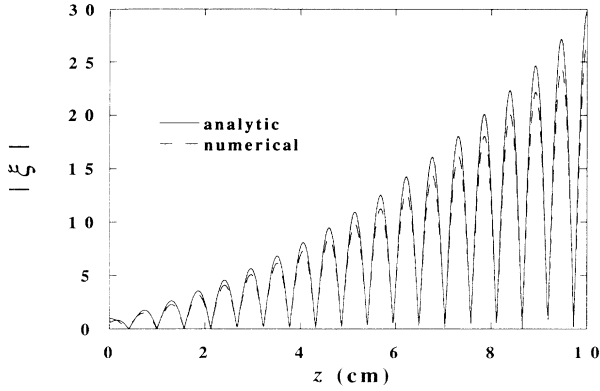


FIG. 14. Comparison of the strong-focusing, short-pulse (“long-range”) asymptotic form of Eq. (23) with the numerical solution for  $Rn_p \sim 1 \times 10^{18} \text{ cm}^{-3}$ ,  $\gamma \sim 1 \times 10^5$ ,  $k_x b \sim 0.3$ ,  $T = 0.05$  ps,  $R = 1$ , and  $\lambda_\beta \sim 1.06$  cm.

In the limit  $\nu \rightarrow 0$ , these results reduce to Eqs. (37) and (38). This result is compared to that obtained numerically in Fig. 15.

In the weak-focusing limit, the stationary points are

$$p_\sigma = -i\sigma\Omega_p - \frac{1}{2}\nu + \left[ \frac{z^2 W_0}{8\gamma\tau^2} \right]^{1/2} \exp \left[ i \frac{\pi\sigma}{6} \right]. \quad (\text{A19})$$

The solution takes the form

$$\xi(z, \tau) \approx \frac{2^{3/2}}{\pi^{1/2} 3^{5/4}} \frac{A^{1/2}}{\Omega_p \tau} \exp \left( A - \frac{1}{2}\nu\tau \right) \times \left\{ \sin \left[ \Omega_p \tau - 3^{-1/2} A - \frac{\pi}{12} \right] - \frac{\nu}{2\Omega_p} \cos \left( \Omega_p \tau - 3^{-1/2} A - \frac{\pi}{12} \right) \right\}, \quad (\text{A20})$$

with the exponent

$$A = \frac{3^{3/2}}{4} \left[ \frac{z^2 \tau W_0}{\gamma} \right]^{1/3}. \quad (\text{A21})$$

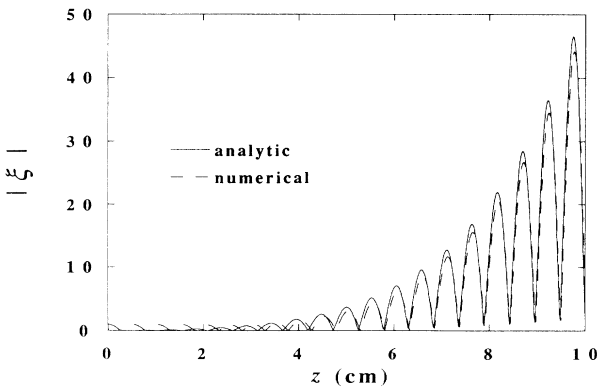


FIG. 15. Comparison of the strong-focusing, long-pulse asymptotic form of Eq. (A17) with the numerical solution for  $Rn_p \sim 1 \times 10^{18} \text{ cm}^{-3}$ ,  $\gamma \sim 1 \times 10^5$ ,  $k_x b \sim 0.3$ ,  $T = 10$  ps,  $R = 30$ , and  $\lambda_\beta \sim 1.06$  cm.

In the limit  $\nu \rightarrow 0$ , these are just Eqs. (18) and (19). This result is compared to the more exact numerical result in Fig. 16.

To compute the asymptotic growth with a distribution in betatron period, we start from Eqs. (41) and (42):

$$\left[ \frac{\partial^2}{\partial \tau^2} + \Omega_p^2 \right] \eta(z, \tau) = \alpha \bar{\xi}(z, \tau), \quad (\text{A22})$$

$$\left[ \frac{\partial^2}{\partial z^2} + \Omega_\beta^2 \right] \xi(z, \tau; \Omega_\beta) = \beta \eta(z, \tau), \quad (\text{A23})$$

where we have abbreviated  $\alpha \equiv \omega_p^2 \rho e^{-\rho} / (1-f)$  and  $\beta = k_p^2 e^{-\rho} / \gamma$ , and  $\bar{\xi}$  is given by Eq. (40). Solving Eq. (A23) up to quadrature and substituting the result in Eq. (A22), we obtain the following results:

$$\left[ \frac{\partial^2}{\partial \tau^2} + \Omega_p^2 \right] \eta(z, \tau) = \alpha \bar{\xi}_{\text{hom}} + \int_0^z dz' G(z-z') \eta(z', \tau), \quad (\text{A24})$$

which is just a beam breakup equation for the centroid of the plasma annulus. The driving term  $\bar{\xi}_{\text{hom}}$  is the homogeneous solution for the beam centroid in the absence of interaction, which is just

$$\bar{\xi}_{\text{hom}} = \int d\Omega_\beta g(\Omega_\beta) \cos(\Omega_\beta z), \quad (\text{A25})$$

assuming a unit initial offset. The kernel is

$$G(z) = \Omega_p^2 k_\beta^2 \Delta^2 \int d\Omega_\beta g(\Omega_\beta) \frac{\sin(\Omega_\beta z)}{\Omega_\beta}. \quad (\text{A26})$$

Laplace transforming in  $z$ , the solution for the plasma flute amplitude is then

$$\bar{\eta}(q, \tau) = \frac{\alpha \bar{\xi}_{\text{hom}}(q)}{\Omega_p^2 - \bar{G}(q)} \{ 1 - \cos[(\Omega_p^2 - \bar{G}(q))^{1/2} \tau] \}. \quad (\text{A27})$$

where  $q$  is the Laplace-transform variable and the tilde denotes the Laplace transform. Substituting from the Laplace-transformed version of Eq. (A22), the solution for the beam flute amplitude is

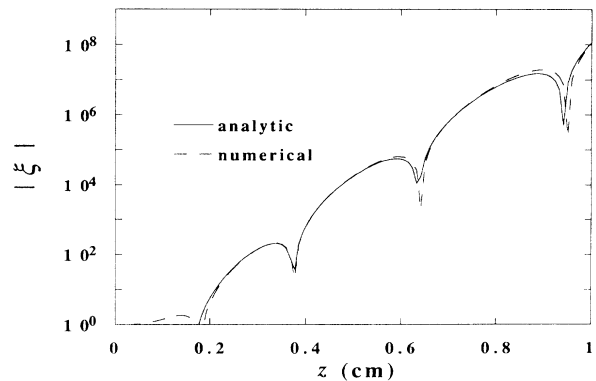


FIG. 16. Comparison of the weak-focusing, long-pulse asymptotic form of Eq. (A20) with the numerical solution for  $Rn_p \sim 1 \times 10^{18} \text{ cm}^{-3}$ ,  $\gamma \sim 1 \times 10^5$ ,  $k_x b \sim 0.3$ ,  $T = 10$  ps,  $R = 1$ , and  $\lambda_\beta \sim 1.06$  cm.

$$\begin{aligned} \tilde{\xi}(q, \tau) = & \tilde{\xi}_{\text{hom}}(q) \frac{\tilde{G}(q)}{\tilde{G}(q) - \Omega_p^2} \cos[(\Omega_p^2 - \tilde{G}(q))^{1/2} \tau] \\ & + \tilde{\xi}_{\text{hom}}(q) \frac{\Omega_p^2}{\Omega_p^2 - \tilde{G}(q)}. \end{aligned} \quad (\text{A28})$$

The last term does not contribute to exponential growth and will be neglected. Performing the inverse Laplace transform, we obtain

$$\begin{aligned} \xi(z, \tau) \approx & \frac{1}{2\pi i} \int_{-i\infty+0^+}^{+i\infty+0^+} dq \exp(qz) \tilde{\xi}_{\text{hom}}(q) \frac{\tilde{G}(q)}{\tilde{G}(q) - \Omega_p^2} \\ & \times \cos[(\Omega_p^2 - \tilde{G}(q))^{1/2} \tau]. \end{aligned} \quad (\text{A29})$$

This may be expressed as  $\xi = (\xi_+ + \xi_-)/2$ , where

$$\xi_\sigma(z, \tau) = \frac{1}{2\pi i} \int_{-i\infty+0^+}^{+i\infty+0^+} dq \psi(q) \exp\{\varphi_\sigma(z, \tau, q)\}, \quad (\text{A30})$$

with  $\sigma = \pm 1$  and

$$\varphi_\sigma(z, \tau, p) = qz + i\sigma(\Omega_p^2 - \tilde{G}(q))^{1/2} \tau. \quad (\text{A31})$$

The algebraic factor is

$$\psi(q) = \tilde{\xi}_{\text{hom}}(q) \frac{\tilde{G}(q)}{\tilde{G}(q) - \Omega_p^2}, \quad (\text{A32})$$

where

$$\tilde{G}(q) = \Omega_p^2 k_\beta^2 \Delta^2 \int d\Omega_\beta \frac{g(\Omega_\beta)}{\Omega_\beta^2 + q^2}, \quad (\text{A33})$$

$$\tilde{\xi}_{\text{hom}}(q) = q \int d\Omega_\beta \frac{g(\Omega_\beta)}{\Omega_\beta^2 + q^2}. \quad (\text{A34})$$

We proceed with a steepest-descent calculation of the integral in Eq. (A28) for the two distributions considered in Sec. III. It is convenient to define  $p = i\sigma(\Omega_p^2 - \tilde{G}(q))^{1/2}$ , so that the dispersion relation, Eq. (43), may be written as  $\Omega_p^2 + p^2 = \tilde{G}(q)$  and the exponent  $\varphi_\sigma(z, \tau, p) = qz + p\tau$ .

First, consider the flat distribution, for which the dispersion relation is

$$\Omega_p^2 + p^2 = \Omega_p^2 \frac{\Delta^2}{2i\delta} \frac{k_\beta}{q} \ln \left\{ \frac{q + i\Omega_+}{q - i\Omega_+} \frac{q - i\Omega_-}{q + i\Omega_-} \right\}. \quad (\text{A35})$$

Considering only the long-pulse, strong-focusing limit, we look for a stationary point such that  $p = i\sigma\Omega_p(1 + \hat{p})$ , and  $q = -i\sigma k_\beta(1 + \hat{q})$ , with  $\hat{p}$  and  $\hat{q}$  small in modulus. The dispersion relation then takes the form

$$\hat{p} = \frac{1}{4} \frac{\Delta^2}{\delta} \ln \left[ 1 + \frac{\delta}{\hat{q}} \right] + \frac{1}{8} \Delta^2. \quad (\text{A36})$$

The equation for the stationary point is then

$$\frac{d\hat{p}}{d\hat{q}} = \frac{k_\beta z}{\Omega_p \tau}, \quad (\text{A37})$$

which is just a quadratic in  $y$ , with the solution

$$\hat{q} = \frac{\delta}{2} \left\{ -1 \pm \left[ 1 - \frac{\Delta^2}{\delta^2} \left[ \frac{\Omega_p \tau}{k_\beta z} \right] \right]^{1/2} \right\}. \quad (\text{A38})$$

To observe growth, we must have  $\text{Re}(\hat{q}) > 0$ , which is evidently possible for small enough  $z$ , where  $\hat{q}z \propto \sqrt{sz}$ , and one recovers the result of Eq. (A18). However, for

$$k_\beta z > \frac{\Delta^2}{\delta^2} \Omega_p \tau, \quad (\text{A39})$$

$\text{Re}(\hat{q}) = 0$ , and growth has saturated. This is just the condition  $z > L_{\text{sat}}$ , with  $L_{\text{sat}}$  as given by Eq. (51). The real part of the exponent at saturation is just

$$\text{Re}(\varphi) = \frac{\pi}{4} \frac{\Delta^2}{\delta} \Omega_p \tau, \quad (\text{A40})$$

and this is just the exponent in Eq. (53). To obtain the remaining algebraic factors in Eq. (52), one must note that the saturation point is also an inflection point for the phase  $\varphi$ ,  $\varphi^{(2)}(q_0) = 0$ , so that the asymptotic form for the integral in Eq. (A28) is not Eq. (A5), but

$$\xi_\sigma \approx \frac{\Gamma(\frac{1}{3})}{2^{2/3} 3^{1/6} \pi [\varphi_\sigma^{(3)}(q_\sigma)]^{1/3}} \psi(q_\sigma) \exp\{\varphi_\sigma(q_\sigma)\}. \quad (\text{A41})$$

Here,  $\Gamma$  is the  $\Gamma$  function, so that  $\Gamma(\frac{1}{3}) \sim 2.6789$ . Comparison of the resulting analytic expression, Eq. (52), with numerical results is seen in Fig. 17.

Next, we consider the parabolic distribution. Solving Eqs. (43), (64), and (65), one can show that  $\text{Im}(\omega)$  has a (finite) maximum  $\omega_m$  on the real  $k_z$  axis. The solution for  $\omega_m$  as a function of  $R$  for  $a = d$  is depicted in Fig. 18, overlaid with the fit

$$\frac{\omega_m}{\omega_p} \approx 1.305(R - 1)^{-0.6062 - 0.03769 \ln(R - 1)}. \quad (\text{A42})$$

For  $R > 10$ , this is roughly  $\omega_m \sim \Omega_p \Delta^2 / \delta$ . This yields an accurate estimate of the log of the saturated amplitude,

$$\ln \xi = A_{\text{sat}} \sim \omega_m \tau + \dots$$

The simplest method of obtaining the algebraic factors is to match this solution to the asymptotic form of Eq. (37), which is accurate for  $z$  sufficiently small that phase mixing is negligible. Equating the exponent of Eq. (38),  $A_3 \sim \omega_m \tau$ , yields an estimate of the scale length for saturation:

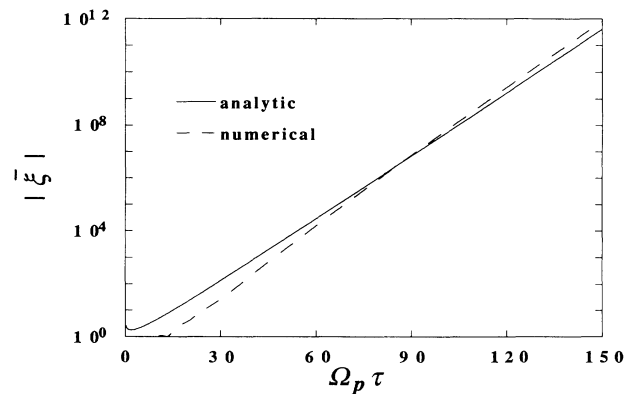


FIG. 17. Comparison of the analytic results, Eqs. (51)–(53), and the numerical solution, for saturation amplitude, with a flat betatron distribution, as in Eq. (49). Parameters are  $\delta = 10\%$ ,  $R n_p = 10^{18} \text{ cm}^{-3}$ ,  $R = 30$ ,  $k_x b \sim 0.3$ , and  $T = 30 \text{ ps}$ .

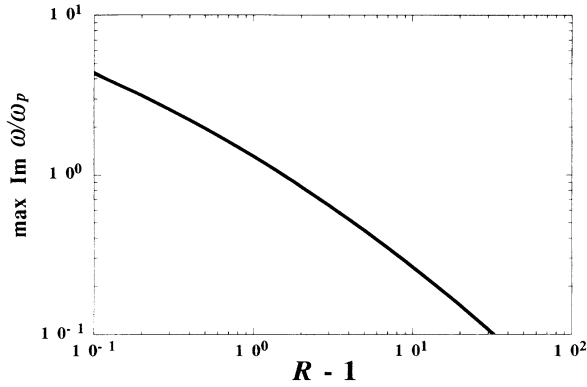


FIG. 18. Several solutions of the dispersion relation, Eqs. (43), (64), and (65), have been collated to depict the maximum of  $\text{Im}(\omega)$  over real  $k_z$  as a function of  $R$ , with  $a/d=1$  and  $k_x b \sim 0.3$  fixed. Overlaid is the (indistinguishable) fit of Eq. (A42).

$$k_{\beta z} \approx 2\Omega_p \tau \frac{1}{\Delta^2} \frac{\omega_m^2}{\Omega_p^2} \approx 2\Omega_p \tau \frac{\Delta^2}{\delta^2}, \quad (\text{A43})$$

which is just the result given in Eq. (44). The amplitude at saturation should then be well approximated by

$$\xi \approx 0.2 \frac{\omega_m}{\Omega_p} \frac{1}{A_{\text{sat}}^{1/2}} \exp(A_{\text{sat}}). \quad (\text{A44})$$

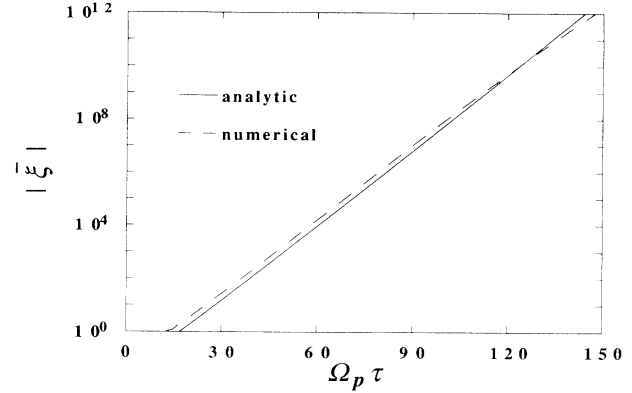


FIG. 19. Comparison of the analytic estimate of Eq. (A44), and the numerical solution amplitude, with a parabolic channel betatron distribution, as in Eq. (61). Parameters are  $Rn_p = 10^{18} \text{ cm}^{-3}$ ,  $R=30$ ,  $k_x b \sim 0.3$ , and  $T=30 \text{ ps}$ . The corresponding spread is  $\delta \sim 13\%$ , and the maximum growth rate is  $\omega_m \sim 0.22\Omega_p$ , which is just the slope of the curves.

Comparison with numerical results depicted in Fig. 19 is seen to be quite good. This simulation was run for 100 betatron periods, which was not quite long enough for the tail to reach saturation, as is evident in the slight droop at large  $\tau$ .

[1] G. I. Budker, in *Proceedings of the CERN Symposium on High Energy Accelerators and Pion Physics* (CERN Service d'Information, Geneva, 1956), pp. 68–75.  
[2] H. L. Buchanan, *Phys. Fluids* **30**, 221 (1987).  
[3] W. E. Martin, G. J. Caporaso, W. M. Fawley, D. Prosnitz, and A. G. Cole, *Phys. Rev. Lett.* **54**, 685 (1985); G. J. Caporaso, F. Rainer, W. E. Martin, D. S. Prono, and A. G. Cole, *ibid.* **57**, 13 (1986).  
[4] R. F. Schneider and J. R. Smith, *Phys. Fluids* **29**, 3917 (1986).  
[5] R. L. Carlson, S. W. Downey, and D. C. Moir, *J. Appl. Phys.* **61**, 12 (1987).  
[6] R. F. Lucey, Jr., R. M. Gilgenbach, J. E. Tucker, and C. L. Enloe, *Laser Part. Beams* **6**, 687 (1988); R. F. Lucey, Jr., R. M. Gilgenbach, J. D. Miller, J. E. Tucker, and R. A. Bosch, *Phys. Fluids B* **1**, 430 (1989).  
[7] J. R. Smith, I. R. Shokair, K. W. Struve, E. Schamiloglu, P. W. Werner, and R. J. Lipinski, *IEEE Trans. Plasma Sci.* **19**, 850 (1991).  
[8] T. Ozaki, K. Ebihara, S. Hiramatsu, Y. Kimura, J. Kishiro, T. Monaka, K. Takayama, and D. H. Whittum, *Nucl. Instrum. Methods A* **318**, 101 (1992).  
[9] J. J. Su, T. Katsouleas, J. M. Dawson, and R. Fedeles, *Phys. Rev. A* **41**, 3321 (1990).  
[10] P. Chen, K. Oide, A. M. Sessler, and S. S. Yu, *Phys. Rev. Lett.* **64**, 1231 (1990).  
[11] W. A. Barletta, in *Proceedings of the Workshop on New Developments in Particle Acceleration Techniques* (CERN Service d'Information, Orsay, 1987), p. 544.  
[12] R. J. Briggs, *Phys. Rev. Lett.* **54**, 2588 (1985).  
[13] J. B. Rosenzweig, B. Breizman, T. Katsouleas, and J. J. Su, *Phys. Rev. A* **44**, 6189 (1991).  
[14] R. B. Palmer, in *New Developments in Particle Acceleration*

*Techniques*, edited by S. Turner (CERN, Geneva, 1987), Vol. 1, pp. 80–120.  
[15] P. Chen, *Phys. Rev. A* **45**, 3398 (1992).  
[16] J. D. Miller, R. F. Schneider, D. J. Weidman, H. S. Uhm, and K. T. Nguyen, *Phys. Rev. Lett.* **67**, 1747 (1991).  
[17] D. H. Whittum, W. M. Sharp, S. S. Yu, M. Lampe, and G. Joyce, *Phys. Rev. Lett.* **67**, 991 (1991).  
[18] M. Lampe, G. Joyce, and S. P. Slinker (unpublished).  
[19] J. D. Lawson, *The Physics of Charged-Particle Beams* (Oxford University Press, Oxford, 1977), pp. 384–387.  
[20] L. J. Laslett, D. Mohl, and A. M. Sessler, in *Proceedings of the Third All-Union National Conference on Particle Accelerators*, Moscow, 1972 (unpublished), reprinted in *Selected Works of L. Jackson Laslett*, Publication 616 (Lawrence Berkeley Laboratory, Berkeley, 1987), pp. 4.96–4.111.  
[21] Implicit in the geometry of Fig. 1 is the assumption  $a_x/b \gg n_b/n_p$ , where  $a_x$  is the beam width in  $x$ .  
[22] O. Buneman, *Phys. Rev.* **115**, 503 (1959).  
[23] R. J. Briggs, *Electron Stream Interaction with Plasmas*, Research Monograph No. 29 (MIT, Cambridge, 1964).  
[24] R. J. Briggs, in *Research Laboratory of Electronics, MIT, Quarterly Progress Report No. 85* (unpublished), pp. 183–185.  
[25] A. Bers, in *Handbook of Plasma Physics*, edited by M. N. Rosenbluth and R. Z. Sagdeev, Basic Plasma Physics I Vol 1 (North-Holland, Amsterdam, 1983), pp. 451–517.  
[26] L. Hall and W. Heckrotte, *Phys. Rev.* **166**, 120 (1968).  
[27] K. L. F. Bane, *Physics of Particle Accelerators*, edited by Melvin Month and Margaret Dienes, AIP Conf. Proc. No. **153** (AIP, New York, 1987), pp. 972–1012.  
[28] Alexander W. Chao, *Physics of High Energy Particle Accelerators*, edited by Melvin Month, AIP Conf Proc. No.

- 105 (AIP, New York, 1983), pp. 353–523.
- [29] This also may be expressed in terms of a coupling impedance per unit length  $r_1$ , as  $W(k_x) = (I/I_0)r_1\Omega_p^2$ , where  $I_0 = mc^3/e \sim 17$  kA and  $I$  is the beam current.
- [30] Y. Y. Lau, Phys. Rev. Lett. **63**, 1141 (1989).
- [31] A. W. Chao, B. Richter, and C. Y. Yao, Nucl. Instrum. Methods **178**, 1 (1980).
- [32] The integro-differential equation is solved numerically using a fourth-order Runge-Kutta advance in  $z$  and a second-order integration in  $\tau$  of the wake-field driving term: *Handbook of Mathematical Functions*, edited by M. Abramowitz and I. A. Stegun (Dover, New York, 1972).
- [33] V. E. Balakin, A. V. Novokhatsky, and V. P. Smirnov, *Proceedings of the Twelfth International Conference on High-Energy Accelerators*, edited by F. T. Cole and R. Donaldson (Fermi National Accelerator Laboratory, Batavia, IL, 1984), pp. 119–120.
- [34] R. J. Alder, B. B. Godfrey, M. M. Campbell, D. J. Sullivan, and T. C. Genoni, Part. Accel. **13**, 25 (1983).
- [35] V. K. Neil, L. S. Hall, and R. K. Cooper, Part. Accel. **9**, 213 (1979).
- [36] This is essentially a “distributed-mass” model analogous to that considered in E. P. Lee, Phys. Fluids **21**, 1327 (1978).
- [37] Note that this model neglects coupling of different flute wave numbers, which may result in additional phase mixing and reduction in growth.
- [38] L. Landau, J. Phys. (Moscow) **10**, 25 (1946).
- [39] Additional discussion of such cutoff (and possible discontinuous) distributions can be found in J. Canosa, J. Gazdag, J. Fromm, and B. H. Armstrong, Phys. Fluids **15**, 2299 (1972), and B. B. Godfrey and B. S. Newberger, *ibid.* **19**, 342 (1976).
- [40] I. S. Gradshteyn and I. M. Ryzhik, *Table of Integrals, Series and Products* (Academic, New York, 1980).
- [41] The approximate form errs at  $O(\mu^4)$  in the limit  $\mu \ll 1$ , and for maximum  $\mu \sim 1/\sqrt{6}$ ,  $\Omega_\beta(\mu)/\Omega_\beta(0) \sim 0.866$  versus 0.864 for the exact result.
- [42] S. Jordan, A. Ben-Amar Baranga, G. Benford, D. Tzach, and K. Kato, Phys. Fluids **28**, 366 (1985).
- [43] Note that in the extreme limit (not considered here)  $v/\omega_p > \sqrt{2}$ , all flute modes are overdamped.
- [44] V. K. Neil and R. K. Cooper, Part. Accel. **1**, 111 (1970).
- [45] M. Lampe, W. Sharp, R. F. Hubbard, E. P. Lee, and R. J. Briggs, Phys. Fluids **27**, 2921 (1984).
- [46] E. J. Lauer, R. J. Briggs, T. J. Fessenden, R. E. Hester, and E. P. Lee, Phys. Fluids **21**, 1344 (1978).
- [47] W. K. H. Panofsky and M. Bander, Rev. Sci. Instrum. **39**, 206 (1968).
- [48] P. C. de Jagher, F. W. Sluijter, and H. J. Hopman, Phys. Rep. **167**, 177 (1988).
- [49] K. Takayama, Phys. Rev. A **45**, 1157 (1992).

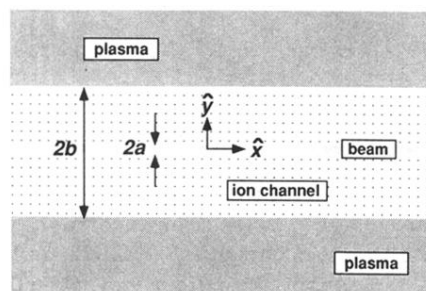


FIG. 1. In equilibrium, a relativistic electron beam of width  $2a$  propagates in the  $z$  direction (out of the page) through a channel of unneutralized ions. Plasma electrons have been expelled to  $|y| \geq b$ .

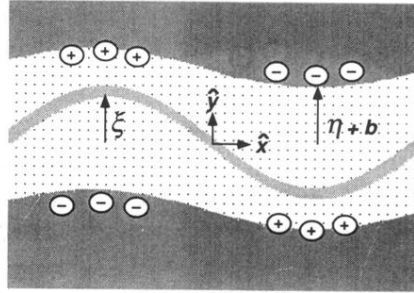


FIG. 2. A beam slice in the ion channel is displaced by an amount  $\xi(x)$  in the  $y$  direction, inducing a displacement  $\eta(x)$  of the channel wall. This image “flute” then deforms follow-on portions of the beam, resulting in instability.

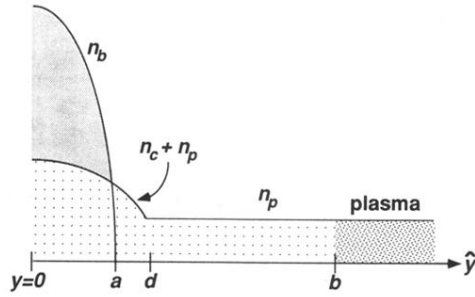


FIG. 5. Finding that propagation in a *uniform* plasma is highly unstable, we consider a *nonuniform* plasma with ion density  $n_i = n_p + n_c$ , where  $n_p$  is constant and  $n_c$  is localized within  $|y| < d$ . We will consider the case of a “flat-top” channel (uniform channel density  $n_c$ ) and a “rounded” channel, as depicted here.